Journal of Innovative Optical Health Sciences
Vol. 11, No. 4 (2018) 1850021 (11 pages)

DOI: 10.1142/S1793545818500219

World Scientific
www.worldscientific.com

Simultaneous quantification of longitudinal and transverse ocular chromatic aberrations with Hartmann–Shack wavefront sensor

Yangchun Deng[*,†,‡,§], Junlei Zhao[*,†,¶], Yun Dai[*,†,‖,††] and Yudong Zhang[*,†,**,††]

[*]*The Key Laboratory on Adaptive Optics*
Chinese Academy of Sciences
Chengdu 610209, P. R. China

[†]*The Laboratory on Adaptive Optics*
Institute of Optics and Electronics
Chinese Academy of Sciences
Chengdu 610209, P. R. China

[‡]*University of Chinese Academy of Sciences*
Beijing 100049, P. R. China
[§]*Missing-y@163.com*
[¶]*hustoejunzuo@163.com*
[‖]*daiyunqq@163.com*
[**]*ydzhang@ioe.ac.cn*

Received 9 January 2018
Accepted 24 April 2018
Published 30 May 2018

A simple method to objectively and simultaneously measure eye's longitudinal and transverse chromatic aberrations was proposed. A dual-wavelength wavefront measurement system using two Hartmann–Shack wavefront sensors was developed. The wavefronts of the red (639.1 nm) and near-infrared (786.0 nm) lights were measured simultaneously for different positions in the model eye. The chromatic wavefronts were converted into Zernike polynomials. The Zernike tilt coefficient (first term) was used to calculate the transverse chromatic aberration along the x-direction, while the Zernike defocus coefficient (fourth term) was used to calculate the longitudinal chromatic aberration. The measurement and simulation data were consistent.

Keywords: Chromatic aberration; Hartmann–Shack wavefront sensor; simultaneity; Zernike coefficient.

[††]Corresponding authors.

1. Introduction

Optic errors of the human eye are divided into monochromatic and chromatic aberrations. Monochromatic-aberration measurements and adaptive optics (AO) aberration correction of the human eye have been performed since 1997.[1] This technique has been widely used in high-resolution retinal imaging and vision studies. According to the geometry, the chromatic aberration can be divided into longitudinal chromatic aberration (or axial chromatic aberration, LCA) and transverse chromatic aberration (or lateral chromatic aberration, TCA). Chromatic aberrations affect the resolution of the multi-wavelength fundus imaging[2–4] and reduce the visual function of a human eye with an intraocular lens (IOL).[5–8] In order to eliminate the negative influence of the chromatic aberrations in multi-wavelength imaging and design of achromatic IOLs,[9,10] it is necessary to study the chromatic aberrations of the human eye.

LCA has been investigated since 1940s. Wald and Griffin employed a specially designed spectral stigmatoscope to measure LCA of the eye using a subjective method. The average LCA between 365 nm and 750 nm was 3.2 D.[11] In 1998, Rynders *et al.* employed a double-pass apparatus to measure the off-axis LCA using both subjective and objective methods in the visible-light range. The average LCA tends to increase gradually between 458 nm and 632.8 nm, from ∼1.0 D at the fovea to approximately 1.6 D at an eccentricity of 40°.[12] In 1999, Marcos *et al.* employed a spatially resolved refractometer to measure the LCA objectively in the visible range. The average LCA between 450 nm and 650 nm was 1.26 D.[13] In their study, unlike in most of the previous approaches based on subjective refraction, LCA was directly objectively estimated. LCA measurements gradually developed from using subjective methods to objective methods. In 2005, Fernández *et al.* used the Hartmann–Shack (HS) wavefront sensor and femtosecond laser to measure LCA in the range of 700–900 nm; the average LCA was 0.4 D.[14] The results of this study are useful in experiments where the chromatic defocus should be corrected including imaging techniques using broadband near-infrared light. In 2008, Manzanera *et al.* employed an HS wavefront sensor and Xe-white-light lamp to measure the LCA (440–694 nm) using an objective method. The average LCA of three subjects was smaller than 2.0 D.[15] Manzanera *et al.* reported that almost all of the systems in use correspond to the latter group; the HS sensor[1,16,17] was standardly used, and the HS wavefront technology became the most common method for LCA measurements. In 2015, Vinas *et al.* studied the discrepancies between the human eye's LCA using both HS wavefront sensor and psychophysics measurement methods. In the range of 488–700 nm, the average LCAs were 1.00 D (objective method) and 1.51 D (subjective method).[18] Studies on LCA achieved a significant progress in terms of number of employed wavelengths, spectral range and measurement methods. However, in many cases, measurements of the LCA did not consider the TCA. In an actual measurement, eye movements[19,20] such as microsaccade, drift and tremor can change the wavefront over time. In all of the current LCA measurement methods, different wavelengths are measured at different times, which inevitably causes a certain amount of measurement error.[21] Vinas *et al.*[18] reported that a simultaneous correction of the eye's chromatic aberrations was necessary, in particular, for applications that require a simultaneous imaging at identical depths with two wavelengths.

The two-color Vernier-alignment technique has been used over a long period of time in TCA measurements. In 1947, Hartridge revealed that when a human eye stared at aligned red and blue sighting marks, the subject would feel that there is an offset between the two sighting marks.[22] The offset between the sighting marks reflects the TCA; the two-color Vernier-alignment technique was developed based on this phenomenon. In 1987, Ogboso *et al.* employed the two-color Vernier-alignment technique to measure TCA between 435 nm and 572 nm using a subjective method. In general, the TCA increased with the retinal eccentricity; however, it remained smaller than 10 arcmin within 40° of the fovea. At 60°, the TCA increased to approximately 30 arcmin.[23] In 1995, Rynders *et al.* used the improved two-dimensional two-color Vernier-alignment technique to measure the TCA between 497 nm and 605 nm, which revealed that the TCA is in the range of 0.05–2.67 arcmin[24]; the two-color Vernier-alignment technique was subjective. The sensitivity of the human eye could decrease in the peripheral visual field; hence, the accuracy of the subjective measurement method would decline. Even if the monochromatic aberrations have been corrected by the AO technique, the resolution acuity of the eye

periphery cannot be improved.[25] Furthermore, the psychophysics measurement method requires the subjects to undergo a measurement training before the experiment, which is time-consuming and cannot guarantee measurement accuracy. Therefore, objective measurements could be advantageous. In 1999, Marcos *et al.* used a spatially resolved refractometer to measure the difference between two alignments, which corresponded to TCAs in different time moments; this method had a lower precision in the estimation of the foveal TCA (0.52–1.84 arcmin) between 473 nm and 601 nm.[13] The influence of the eye movements, in particular that of microsaccades,[26] was significant in the TCA measurement. In this method, each measurement had to be realigned to the reference, which was the main cause of the low precision. This issue can be overcome by a simultaneous measurement of wavefront quantities. In 2016, Winter *et al.* used an adaptive optics scanning laser ophthalmoscope (AOSLO) system to achieve an objective and simultaneous method for TCA measurements across all four visual-field directions in the range of 543–842 nm. The measurement method was based on the Grieve *et al.*'s[3] and Harmening *et al.*'s[4] studies. The TCA increased linearly with the eccentricity, with an average slope of 0.21 arcmin per degree of visual-field angle.[27] However, this system was very complex; in order to measure the TCA, the retina should be imaged and then different-wavelength fundus images should be analyzed.

McLellan *et al.*[28] reported that monochromatic aberration, LCA and TCA interplayed to impact the retinal image quality. A simultaneous LCA and TCA measurement was necessary for a chromatic-aberration study. To the best of our knowledge, methods to simultaneously obtain the two chromatic aberrations (TCA and LCA) have not yet been developed. In this study, two HS wavefront sensors were used to achieve a simultaneous measurement of both chromatic aberrations with two wavelengths. The simultaneous measurement prevented errors attributed with the interplay between the two chromatic aberrations. In addition, it reduced the measurement time and error. Simultaneous measurement technology is indispensable for a higher-precision chromatic-aberration determination.

In this study, a simple method was proposed, based on an objective measurement of TCA and simultaneous measurement of LCA. The chromatic aberrations were calculated using only the measurement data of the eye wavefront. In Sec. 2, the principle of the measurement method is discussed. In Sec. 3, the development of a two-wavelength wavefront measurement system is presented. In Sec. 4, a model eye is proposed, which is used in the experiment. The method of the chromatic-aberration measurement is described in Sec. 5. Measurement results and discussion are provided in Sec. 6. The conclusions of this study are presented in Sec. 7.

2. Principle of the Measurement Method

According to the Thibos *et al.*'s study,[29] the chromatic aberration can be expressed in both object and image spaces (Fig. 1). The two-color Vernier-alignment technique for the measurement of TCA is based on the image space. The measurement of the LCA using the HS wavefront sensor is based on the object space. In this study, HS sensor is employed to measure TCA in the object space [Fig. 1(d)]. The angular difference between the chief rays with different wavelengths can be represented as the overall tilt-angle difference of the wavefronts. For the human eye, the wavefront $W(x, y)$ can be measured using an HS sensor and can be expressed by the Zernike polynomials $Z_i(x, y)$[17,30]:

$$W(x, y) = \sum_i C_i Z_i(x, y), \tag{1}$$

where C_i is the Zernike coefficient, while i is an integer that represents the terms of the Zernike polynomials; $Z_i(x, y)$ is the i th term of the Zernike polynomial.

The chromatic aberration of human eye can be calculated using the Zernike coefficients (Table 1). The LCA can be described as the difference between the Zernike defocus coefficients of different wavelengths. The TCA is equal to the difference between the Zernike tilt coefficients, and it is called Zernike TCA.[31]

The application of double-pass technology is an advancement in the measurements of monochromatic aberration of human eye. When the double-pass system is employed in chromatic experiments, the phenomenon of chromatic-aberration cancellation cannot be ignored,[32,33] as the double-pass imaging process features autocorrelation. The TCA is

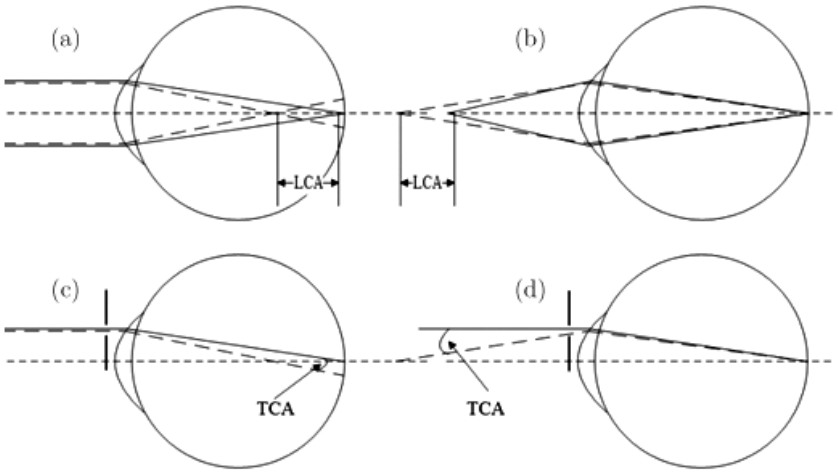

Fig. 1. Illustration of eye's TCA and LCA in the image and object spaces. The dotted line represents red light, while the solid line represents near-infrared light. LCAs in the (a) image and (b) object spaces. TCAs in the (c) image and (d) object spaces.

Table 1. Zernike coefficients, C_0–C_4.

Term	Zernike polynomial	Meaning
C_0	1	Constant term
C_1	$\rho \sin\theta$	Tilt in x-direction
C_2	$\rho \cos\theta$	Tilt in y-direction
C_3	$\rho^2 \sin(2\theta)$	Astigmatism with axes at $\pm$ 45°
C_4	$2\rho^2$–1	Defocus

canceled by the second-pass optic path, when the light passes through the eye's optical system. The entrance and exit pupil (P) sizes can be made unequal to reduce the cancellation to the minimum.[34] In this study, an artificial pupil (AP) is set at the entrance light path to produce diffraction-limited light spots at the retina; the entrance and exit pupils have different sizes to retain the odd-aberration information such as tilt and coma.

3. Description of the Measurement System

Figure 2 illustrates the chromatic-aberration measurement system. Red (THORLABS LP637-SF70, 639.1 nm, LD1) and near-infrared (THORLABS LP785-SF20, 786.0 nm, LD2) light sources were employed. The two LDs were installed on a three-dimensional adjustment rack. Two collimating lenses (L1 and L2) were placed in front of the lasers. Red and near-infrared light beams were emitted from the lasers. The two light beams were collimated by L1 and L2, respectively, and combined by a beam splitter (BS1, Edmund No. 86-395, reflective band: 632.8–647.1 nm, 96%; transmission band: 671.0–790.0 nm, 94%). The two beams passed through an AP and a beam splitter (BS2) reflected the lights that enter into the eye. The two light spots on the retina were separated from each other owing to the TCA. LD1 was adjusted to make the red light spot coincident with the near-infrared light spot. Then, the TCA in the image space was converted into the object space. The two beacons came out of the eye back to the measuring light path, carrying the wavefront information; then, they passed through BS2, were deflected by SM1, M3

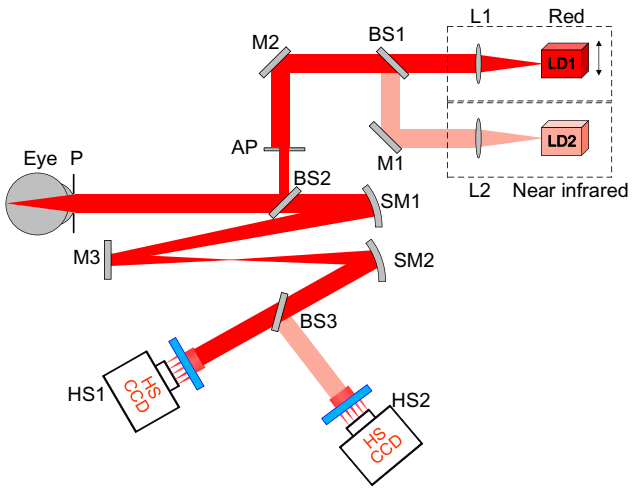

Fig. 2. Illustration of the chromatic-aberration measurement system, which comprises: L: collimating lens, P: pupil of the eye, AP: artificial pupil, BS: beam splitter, SM: spherical mirror and M: plane mirror.

and SM2 and were transmitted to another beam splitter (BS3, Edmund No. 86-395). BS3 was employed to separate the wavefront of the red light received by the HS wavefront sensor 1 (HS1) and that of the near-infrared light received by HS2. Both HS sensors were consisting of a 16×16 microlens array (diameter of each microlens: $400\,\mu$m; focal length: 15 mm) and a CCD camera (Baumer; type: TXG14NIR).

The AP enabled paraxial incidence of the light to avoid specular reflection from the front surface of the model eye. Spherical mirrors (SM1 and SM2) were employed to match the 6-mm diameter of the pupil with the 6.5-mm diameter of the HS wavefront sensors' pupil without introducing an additional chromatic aberration in the system. The SM1 and SM2 were installed in a three-dimensional arrangement to compensate the system's monochromatic aberration, which increased owing to the oblique incidence. Plane mirrors (M1, M2 and M3) were employed to deflect the light path. Two HS sensors were used to prevent an influence of eye movements such as microsaccade, drift and tremor. Therefore, the two simultaneously used HS sensors can maintain the relative value of the chromatic aberration during the measurement process.

4. Design of a Chromatic Eye Model

In order to verify the feasibility of the proposed chromatic-aberration measurement method, a chromatic-aberration eye model was developed. The chromatic-aberration eye model consisted of a plano-convex lens (K9, radius of curvature $R = 51.69$ mm, focal length $F = 100$ mm, back focal length $F_b = 92.7$ mm and center thickness $T_c = 11.0$ mm) and diffuser (diameter $D = 25$ mm, 120-grit THORLABS DG10-120-MD), which simulated the retina, as shown in Fig. 3. A pellicle beam splitter and fundus charge-coupled device (CCD) were used to observe the diffraction-limited light spots. The light spots for the two wavelengths can be observed using the fundus CCD.

In order to verify the accuracy of the chromatic-aberration measurement method, the chromatic-aberration eye model was emulated using the ZEMAX (Radiant Zemax) optical design software. The TCA was calculated along the x-direction. The 639.1-nm and 786.0-nm wavelengths were chosen, consistent with the actual measurement lights.

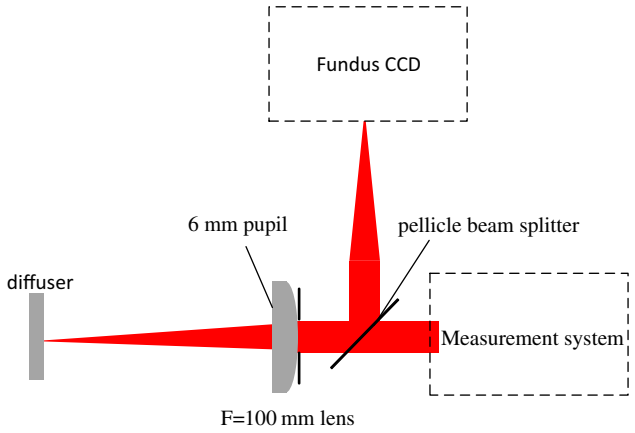

Fig. 3. Illustration of the chromatic-aberration eye model and fundus observation system.

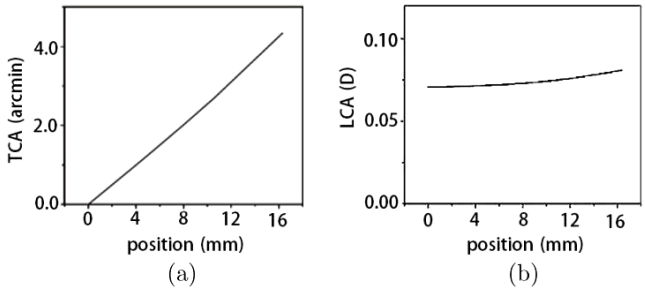

Fig. 4. Dependences of (a) TCA and (b) LCA as a function of the position in the eye model; the zero-position corresponds to the center of the eye model.

The dependences of TCA [Fig. 4(a)] and LCA [Fig. 4(b)] as a function of the measurement position of the eye model are revealed. In Fig. 4, the x-axis represents the position in the eye model, from the center (position 0) to the periphery.

5. Chromatic-Aberration Measurement

5.1. *System control and calibration*

The HS sensors were controlled by a software developed in Visual C++ (Microsoft, USA). The wavefront information for the two wavelengths is displayed on the same computer monitor in real time. The image of the fundus CCD camera was displayed on another computer monitor.

Prior to the experiment, the measurement system was calibrated using standard parallel light sources with the same wavelengths as those of the beacon lights (639.1 nm and 786 nm). The centroids

of the HS sensors' microlens surfaces were calibrated to eliminate the original system's aberration errors.

5.2. *Calculation of the chromatic aberration*

The pupil wavefront information for the two wavelengths were collected simultaneously by different HS sensors. The computer converted the wavefront information into Zernike polynomials: $W(x,y) = \sum_i C_i Z_i(x,y)$; the LCA can be calculated using the expression

$$D = D_r - D_i = 4\sqrt{3}(C_{r4} - C_{i4})/R^2, \qquad (2)$$

where D is the LCA (expressed in diopter), D_r is the red light's defocus, D_i is the near-infrared light's defocus, C_{r4} is the red light's defocus (in μm), C_{i4} is the near-infrared light's defocus (in μm) and R is the pupil radius. The TCA can be calculated using the expression

$$\tan\theta_r - \tan\theta_i = 2C_{r1}R/R - 2C_{i1}/R, \qquad (3)$$

where θ_r is the angle between the measuring axis and red-light chief ray, θ_i is the angle between the measuring axis and near-infrared light chief ray, C_{r1} is the Zernike x-tilt coefficient of the red light and C_{i1} is the Zernike x-tilt coefficient of the near-infrared light. As the measurement angle is sufficiently small, the expression can be approximated as

$$\tan\theta_r - \tan\theta_i \approx \theta_r - \theta_i = \Delta\theta' = 2\Delta C_1'/R, \qquad (4)$$

$$\Delta C_1' = C_{r1} - C_{i1}, \qquad (5)$$

where $\Delta\theta'$ is the TCA expressed in arcmin; $\Delta\theta'$ also represents the overall tilt deviation between the wavefronts of the two wavelengths.

5.3. *Experiments using the eye model*

Six positions between the center and edge of the eye model along the x-direction were selected for the measurement. The fundus light points were displayed for each position. The red LD1 was adjusted to provide coincident light points. Then, the pupil wavefront information were collected by the HS sensors simultaneously in a period of 10 s. The chromatic aberrations were calculated by averaging the data.

The measurement was repeated for each of the selected measurement positions (six positions) of the eye model. Repetitive experiments were performed in three different time periods, and then the data for each measurement position were averaged.

5.4. *Experiments on human eye*

5.4.1. *Subjects*

Two normal subjects (S1: female, aged 27; and S2: male, aged 25) participated in this study. The subjects had no previous history of ocular surgery or trauma and had corrected vision. The measurements were performed for the right (R) and left (L) eyes of S1, and for the right eye of S2. During the experiments, the subjects subjectively judged the coincidence between the two beacons.

In order to avoid a constriction of the human eye pupil, paralysis of accommodation and dilation of pupil were achieved using 1% cyclopentolate. Informed consents were obtained from all subjects. The experiment procedures conformed to the tenets of the Declaration of Helsinki. The power levels of the LDs at the pupil were smaller than 23 μW during the experiment, which was well below the maximum permissible exposure (red: 384.7 μW; near infrared: 571.6 μW) for a continuous viewing established by the American National Standards Institute.[35]

5.4.2. *Experiments*

The subject's head was fixed using a rack. First, the beacon light intensity was adjusted to a comfortable brightness. The subjects subjectively judged the positions of the two beacon points then adjusted the LD1 to obtain coincident light points. Second, the beacon light intensity was adjusted according to the HS sensors' detectable intensity. The pupil wavefront information were collected by the HS sensors' simultaneously in 10 s (20 ms per frame). Third, the untrusted data, affected by blinks, were removed. The chromatic aberrations were calculated by averaging the remaining data. For each eye, the measurements were repeated three times only in the central field of view.

6. Results and Discussion

6.1. *Results of the eye model*

After eliminating the chromatic aberration introduced by the system using the zero-position data (center of the eye model), the two chromatic aberrations of the measured and calculation results are shown in Figs. 5 and 6, respectively; the data are also provided in Tables 2 and 3, respectively.

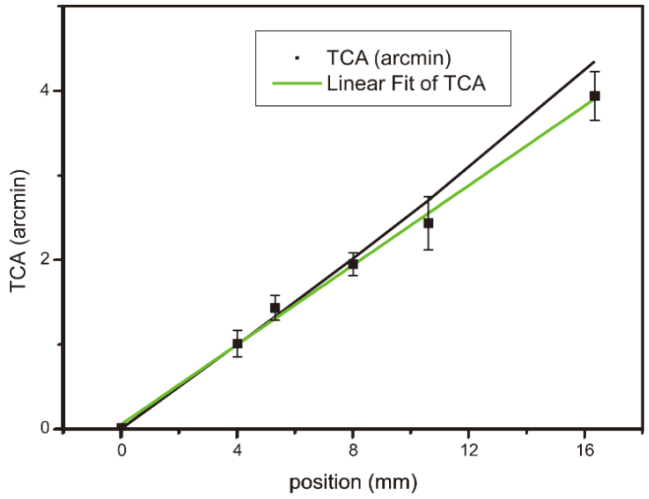

Fig. 5. (Color online) TCA as a function of the position. The black curve represents the calculations, while the green curve represents the fitting of the measured values. The black squares represent the mean TCA values for each measurement position, while the error bars represent the standard deviations.

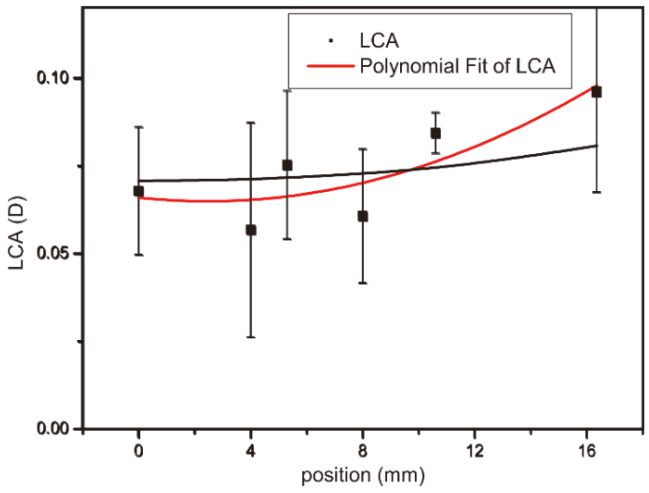

Fig. 6. (Color online) Dependence of the LCA as a function of the position. The black curve represents the calculations, while the red curve represents the fitting of the measured values. The black squares represent the mean values of the LCA for each measurement position, while the error bars represent the standard deviations.

Table 2. Measured and calculated TCA data.

Position (mm)	Measured TCA (arcmin)	Calculated TCA (arcmin)	TCA's standard deviation
0.00	0.000	0.000	0.051
4.00	1.004	0.994	0.156
5.30	1.4278	1.322	0.147
8.00	1.945	2.012	0.135
10.60	2.430	2.699	0.314
16.36	3.937	4.346	0.287

Table 3. Measured and calculated LCA data.

Position (mm)	Measured LCA (D)	Calculated LCA (D)	LCA's standard deviation
0.00	0.067	0.070	0.018
4.00	0.056	0.071	0.030
5.30	0.075	0.071	0.021
8.00	0.060	0.072	0.019
10.60	0.084	0.074	0.005
16.36	0.096	0.080	0.028

The results of the ZEMAX calculations (Fig. 5) showed that the TCA increased monotonously as a function of the position. The standard deviations increased with the off-axis distance, as the monochromatic aberration increased with the off-axis distance.

Figure 6 shows that the LCA was small, close to the measurement accuracy. The measurement data points are near the calculated data points. The standard deviations appearing large were due to the small LCA value itself.

6.2. *Results for the human eye*

Table 4 shows the TCA and LCA results of the three eyes of the two subjects in the central field of view. The average horizontal TCA was 2.496 arcmin, while the vertical TCA was 0.458 arcmin in the central field of view. The average LCA was 0.339 D. All measurement results were repeatable.

These results of chromatic aberration were calculated by the wavefronts which detected from HS sensors. Here, the main HS sensor's measurement errors are repeatability error and accuracy error.[36] Repeatability error of this system was calculated by multiple measurements of the same position of the model eye. Repeatability is expressed in standard deviation of root mean square (RMS). The standard

Table 4. Chromatic aberrations between red (639.1 nm) and near-infrared (786 nm) lights in the central field of view.

Subject	Horizontal TCA (arcmin)	Vertical TCA (arcmin)	LCA (D)
S1 L	2.076 ± 0.153	0.385 ± 0.035	0.334 ± 0.011
S1 R	2.620 ± 0.116	0.237 ± 0.012	0.334 ± 0.033
S2 R	2.792 ± 0.117	0.752 ± 0.278	0.348 ± 0.028
Average	2.496 ± 0.129	0.458 ± 0.108	0.339 ± 0.024

deviation of red light RMS was 0.01 μm. And the standard deviation of near-infrared light RMS was 0.0022 μm. Accuracy error is defined as the ability of the sensor to measure a given known wavefront. The accuracy error of HS sensor was 0.02 μm in this chromatic-aberration measurement system.

6.3. *Discussion*

The model eye experiment demonstrated the feasibility of the proposed method. A primary human eye experiment was performed to demonstrate that the method can also be applied for real human eyes.

Table 5 shows TCA data reported in recent studies. The statistical TCA results significantly varied among the subjects, even between the eyes of the same subject. Rynders *et al.*[24] used the subjective method to measure 85 subjects' eyes for a statistical analysis. The wavelength spacing was 108 nm, between 497 nm and 605 nm. The visual axis TCA was in the range of 0.05–2.67 arcmin. The comparison with Rynders *et al.*'s[24] study shows that our wavelength spacing was 147 nm and that the TCA measurement results (Table 4) were mainly in the range of those provided in their study, which further confirms the reliability of our TCA measurement results.

Table 6 shows LCA data reported in previous studies. The LCA measurements in recent studies focused on the visual-light band, owing to the significant interests in multi-focal (M)-IOL design[9,10] in vision science. Owing to the multi-wavelength fundus imaging, studies were also focused on the infrared light range. In this study, both visible and infrared lights are considered. Previous studies employed different spectral ranges and conditions. It was challenging to compare the measurement results directly. However, the LCA results can be compared with those obtained by the longitudinal chromatic dispersion equations.[37] Atchison and Smith[38] showed that the theoretically derived Cauchy's equation yields results that are in an excellent agreement with the data in the visible spectrum. It can be employed to extrapolate reliable

Table 5. TCA data reported in previous studies.

Study (S: subjective, O: objective)	Number of subjects	Wavelength (nm)	Average visual axis TCA (arcmin)
Rynders *et al.*,[24] 1995 (S)	85	497–605	0.05–2.67
Marcos *et al.*,[13] 1999 (O)	2	473–601	0.52–1.84
Grieve *et al.*,[3] 2006 (O)	3	532–840	1.41–3.68
Winter *et al.*,[27] 2016 (O)	4	543–842	∼2.00
This study (O)	2	639.1–786	2.10–2.80

Table 6. LCA data reported in previous studies.

Study (S: subjective, O: objective)	Number of subjects	Wavelength (nm)	Average visual axis LCA (D)
Wald and Griffin,[11] 1947 (S)	21	365–750	3.2
Rynders *et al.*,[12] 1998 (O)	4	458–632.8	1.0
Marcos *et al.*,[13] 1999 (O)	3	450–650	1.26
Fernández *et al.*,[14] 2005 (O)	4	700–900	0.4
Manzanera *et al.*,[15] 2008 (O)	3	440–694	∼1.75
Vinas *et al.*,[18] 2015 (O)	5	488–700	1.00
Vinas *et al.*,[18] 2015 (S)	5	488–700	1.51
Vinas *et al.*,[18] 2015 (O)	5	700–950	0.45
This study (O)	2	639.1–786	0.34

results in the nearinfrared range:

$$R_X(\lambda) = 1.60911 - 6.70941 \times 10^5/\lambda^2 + 5.55334 \times 10^{10}/\lambda^4 - 5.59998 \times 10^{15}/\lambda^6, \quad (6)$$

where $R_x(\lambda)$ is the LCA between λ and 590 nm. In this study, using the Cauchy's equation, LCA, calculated between 639.1 nm and 786 nm, was 0.428 D (compared with the LCA measurement value of 0.34 D). The Cauchy's equation was based on psychophysical measurement data which was a subjective method. However, the results of our LCA were obtained by an objective method. Vinas *et al.*[18] indicated that the psychophysically measured LCA was significantly higher than the value obtained using HS technique which was an objective method. The results of our LCA measurement were lower than the calculated results. Measured results and the calculated results of LCA were consistent with this phenomenon.

Current chromatic-aberration measurements are performed by 2–5 subjects to verify the feasibility of the experiment. Two subjects (three eyes) were chosen in our study to demonstrate the feasibility of the method.

This system was originally designed for the measurement of chromatic aberrations of human eye in large visual field. First, subjects were asked to distinguish fundus color spots. Owing to the monochromatic aberrations, in particular, spherical aberration, coma and astigmatism, in real human eye, the fundus color spots were too blurry to be distinguished, in particular, in the peripheral vision. Then, the experiment operator analyzed the fundus color spots through the fundus camera to improve accuracy. However, the monochromatic aberrations affect the quality of the fundus spots. In the peripheral field of the eye, the blurring is worse. Therefore, the real-human-eye experiment in large visual field was unsatisfactory. The experiments can be performed for the eye with a low monochromatic aberration in the central field of view, which demonstrated that the chromatic-aberration measurement method is feasible.

Clear eyes' point spread function (PSF) can be obtained using the AO technology. Further studies are required to complement the AO technique to enable chromatic-aberration measurements for human eye in entire visual field. In the future, according to the type of practical application, corresponding number of wavelengths can be used to enrich the chromatic-aberration information. The distance between the fundus color spot and measuring fundus axis cannot be obtained from the camera image. Therefore, the TCA in the image space cannot be calculated without the distance data. Only approximate values can be obtained by calculations. A more accurate TCA still needs to be obtained using HS sensors in the object space.

7. Conclusion

A system for an objective and simultaneous measurement of chromatic aberrations of human eye was presented. Images of the retina and measurement trainings of the subjects were not required. The chromatic-aberration measurement can provide more accurate chromatic-aberration data for a personalized human eye model design. Regarding clinical applications, the chromatic-aberration data could optimize the design of IOL. For fundus photography applications, the measured chromatic-aberration data can be employed to compensate the multi-wavelength image chromatic-aberrations of the eye in real time. After the compensation, high-definition fundus images can be obtained. This technique can also be employed to evaluate the chromatic aberration of a lens.

Acknowledgments

This work was funded by National Science Foundation of China (NSFC) (61378064) and the National High Technology Research and Development Program of China (2015AA020510).

References

1. J. Liang, D. R. Williams, D. T. Miller, "Supernormal vision and high-resolution retinal imaging through adaptive optics," *J. Opt. Soc. Am. A* **14**(11), 2884–2892 (1997).
2. F. Reinholz, R. A. Ashman, R. H. Eikelboom, "Simultaneous three wavelength imaging with a scanning laser ophthalmoscope," *Cytometry* **37**(3), 165–170 (1999).
3. K. Grieve, P. Tiruveedhula, Y. Zhang, A. Roorda, "Multi-wavelength imaging with the adaptive optics scanning laser ophthalmoscope," *Opt. Express* **14**(25), 12230–12242 (2006).
4. W. M. Harmening, P. Tiruveedhula, A. Roorda, "Measurement and correction of transverse

chromatic offsets for multi-wavelength retinal microscopy in the living eye," *Biomed. Opt. Express* **3**(9), 2066–2077 (2012).
5. K. Ohnuma, H. Kayanuma, T. Lawu, K. Negishi, T. Yamaguchi, T. Noda, "Retinal image contrast obtained by a model eye with combined correction of chromatic and spherical aberrations," *Biomed. Opt. Express* **2**(6), 1443–1457 (2011).
6. P. Pérez-Merino, C. Dorronsoro, L. Llorente, S. Durán, I. Jiménez-Alfaro, S. Marcos, "*In vivo* chromatic aberration in eyes implanted with intraocular lenses," *Invest. Ophthalmol. Vis. Sci.* **54**(4), 2654–2661 (2013).
7. M. Nakajima, T. Hiraoka, T. Yamamoto, S. Takagi, Y. Hirohara, T. Oshika, T. Mihashi, "Differences of longitudinal chromatic aberration (LCA) between eyes with intraocular lenses from different manufacturers," *PLoS ONE* **11**(6), e0156227 (2016).
8. M. Vinas, C. Dorronsoro, N. Garzon, F. Poyales, S. Marcos, "*In vivo* subjective and objective longitudinal chromatic aberration after bilateral implantation of the same design of hydrophobic and hydrophilic intraocular lenses," *J. Cataract. Refract. Surg.* **41**(10), 2115–2124 (2015).
9. M. A. Gil *et al.*, "Comparison of far and near contrast sensitivity in patients symmetrically implanted with multifocal and monofocal IOLs," *Eur. J. Ophthalmol.* **24**(1), 44–52 (2013).
10. W. W. Hütz, R. Jäckel, P. C. Hoffman, "Comparison of visual performance of silicone and acrylic multifocal IOLs utilizing the same diffractive design," *Acta Ophthalmol.* **90**(6), 530–533 (2012).
11. G. Wald, D. R. Griffin, "The change in refractive power of the human eye in dim and bright light," *J. Opt. Soc. Am.* **37**(5), 321–336 (1947).
12. M. C. Rynders, R. Navarro, M. A. Losada, "Objective measurement of the off-axis longitudinal chromatic aberration in the human eye," *Vis. Res.* **38**(4), 513–522 (1998).
13. S. Marcos, S. A. Burns, E. Moreno-Barriusop, R. Navarro, "A new approach to the study of ocular chromatic aberrations," *Vis. Res.* **39**(26), 4309–4323 (1999).
14. E. Fernández, A. Unterhuber, P. Prieto, B. Hermann, W. Drexler, P. Artal, "Ocular aberrations as a function of wavelength in the near infrared measured with a femtosecond laser," *Opt. Express* **13**(2), 400–409 (2005).
15. S. Manzanera, C. Canovas, P. M. Prieto, P. Artal, "A wavelength tunable wavefront sensor for the human eye," *Opt. Express* **16**(11), 7748–7755 (2008).
16. P. M. Prieto, F. Vargas-Martin, S. Goelz, P. Artal, "Analysis of the performance of the Hartmann–Shack sensor in the human eye," *J. Opt. Soc. Am. A* **17**, 1388–1398 (2000).
17. J. Liang, B. Grimm, S. Goelz, J. F. Bille, "Objective measurement of wave aberrations of the human eye with the use of a Hartmann–Shack wavefront sensor," *J. Opt. Soc. Am. A* **11**(7), 1949–1957 (1994).
18. M. Vinas, C. Dorronsoro, D. Cortes, D. Pascual, S. Marcos, "Longitudinal chromatic aberration of the human eye in the visible and near infrared from wavefront sensing, double-pass and psychophysics," *Biomed. Opt. Express* **6**(3), 948–962 (2015).
19. J. Otero-Millan, X. G. Troncoso, S. L. Macknik, I. Serrano-Pedraza, S. Martinez-Conde, "Saccades and microsaccades during visual fixation, exploration, and search: Foundations for a common saccadic generator," *J. Vis.* **8**(14), 21-1–21-18 (2008).
20. S. Martinez-Conde, S. L. Macknik, "Fixational eye movements across vertebrates: Comparative dynamics, physiology, and perception," *J. Vis.* **8**(14), 28-1–28-16 (2008).
21. B. Jaeken, L. Lundström, P. Artal, "Peripheral aberrations in the human eye for different wavelengths: off-axis chromatic aberration," *J. Opt. Soc. Am. A* **28**(9), 1871–1879 (2011).
22. H. Hartridge, "The visual perception of fine detail," *Philos. Trans. R. Soc. B, Biol. Sci.* **232**, 519–671 (1947).
23. Y. U. Ogboso, H. E. Bedell, "Magnitude of lateral chromatic aberration across the retina of the human eye," *J. Opt. Soc. Am. A* **4**(8), 1666–1672 (1987).
24. M. Rynders, B. Lidkea, W. Chisholm, "Statistical distribution of foveal transverse chromatic aberration, pupil centration, and angle Ψ in a population of young adult eyes," *J. Opt. Soc. Am. A* **12**(10), 2348–2357 (1995).
25. L. Lundström *et al.*, "Effect of optical correction and remaining aberrations on peripheral resolution acuity in the human eye," *Opt. Express* **15**(20), 12654–12661 (2007).
26. S. Martinez-Conde, S. L. Macknik, X. G. Troncoso, D. H. Hubel, "Microsaccades: A neurophysiological analysis," *Trends Neurosci.* **32**(9), 463–475 (2009).
27. S. Winter *et al.*, "Transverse chromatic aberration across the visual field of the human eye," *J. Vis.* **16**(14), 9 (2016).
28. J. S. McLellan, S. Marcos, P. M. Prieto, S. A. Burns, "Imperfect optics may be the eye's defence against chromatic blur," *Nature* **417**(9), 174–176 (2002).
29. L. N. Thibos, A. Bradley, D. L. Still, X. Zhang, P. A. Howarth, "Theory and measurement of ocular chromatic aberration," *Vis. Res.* **30**(1), 33–49 (1990).

30. G. M. Dai, Ocular wavefront sensing and reconstruction, *Wavefront Optics for Vision Correction*, pp. 97–119, SPIE Press, Bellingham (2008).
31. J. Nam, J. Rubinstein, L. Thibos, "Wavelength adjustment using an eye model from aberrometry data," *J. Opt. Soc. Am. A* **27**(7), 1561–1574 (2010).
32. P. Artal, S. Marcos, D. R. Williams, R. Navarro, "Odd aberrations and double-pass measurements of retinal image quality," *J. Opt. Soc. Am. A* **12**(2), 195–201 (1995).
33. A. Guirao, N. Lopez-Gil, P. Artal, Double-pass measurements of retinal image quality: A review of the theory, limitations and results, *Proc. 2000 Conf. Vision Science and its Applications*, Optical Society of America, Washington, DC (2000).
34. P. Artal, I. C. Iglesias, N. Lopez-Gil, "Double pass system with unequal entrance and exit pupil sizes to measure the optical transfer function of the human eye," *Proc. SPIE* **2632**, 56–61 (1996).
35. Laser Institute of America, ANSI Standard Z136.1: American National Standard for the Safe Use of Lasers (2014).
36. D. R. Neal, J. Copland, D. A. Neal, "Shack-Hartmann wavefront sensor precision and accuracy," *Proc. SPIE* **4779**, 148–160 (2002).
37. L. N. Thibos, M. Ye, X. Zhang, A. Bradley, "The chromatic eye: A new reduced-eye model of ocular chromatic aberration in humans," *Appl. Opt.* **31**(19), 3594–3600 (1992).
38. D. A. Atchison, G. Smith, "Chromatic dispersions of the ocular media of human eyes," *J. Opt. Soc. Am. A* **22**(1), 29–37 (2005).